
Quantitative PET of Human Urokinase-Type Plasminogen Activator Receptor with ^{64}Cu -DOTA-AE105: Implications for Visualizing Cancer Invasion

Morten Persson¹⁻⁴, Jacob Madsen², Søren Østergaard⁵, Mette Munk Jensen^{2,3}, Jesper Tranekjær Jørgensen^{2,3}, Karina Juhl⁴, Charlotte Lehmann⁴, Michael Ploug^{1,4}, and Andreas Kjaer¹⁻³

¹The Danish Chinese Center for Proteases and Cancer, Copenhagen, Denmark; ²Department of Clinical Physiology, Nuclear Medicine and PET, Rigshospitalet, Copenhagen, Denmark; ³Cluster for Molecular Imaging, Faculty of Health Sciences, University of Copenhagen, Copenhagen, Denmark; ⁴Finsen Laboratory, Rigshospitalet, Biocenter, Copenhagen, Denmark; and ⁵Novo Nordisk A/S, Diabetes Protein and Peptide Chemistry, Måløv, Copenhagen, Denmark

Expression levels of the urokinase-type plasminogen activator receptor (uPAR) represent an established biomarker for poor prognosis in a variety of human cancers. The objective of the present study was to explore whether noninvasive PET can be used to perform a quantitative assessment of expression levels of uPAR across different human cancer xenograft models in mice and to illustrate the clinical potential of uPAR PET in future settings for individualized therapy. **Methods:** To accomplish our objective, a linear, high-affinity uPAR peptide antagonist, AE105, was conjugated with DOTA and labeled with ^{64}Cu (^{64}Cu -DOTA-AE105). Small-animal PET was performed in 3 human cancer xenograft mice models, expressing different levels of human uPAR, and the tumor uptake was correlated with the uPAR expression level determined by uPAR enzyme-linked immunosorbent assay. The tumor uptake pattern of this tracer was furthermore compared with ^{18}F -FDG uptake, and finally the correlation between sensitivity toward 5-fluorouracil therapy and uPAR expression level was investigated. **Results:** The uPAR-targeting PET tracer was produced in high purity and with high specific radioactivity. A significant correlation between tumor uptake of ^{64}Cu -DOTA-AE105 and uPAR expression was found ($R^2 = 0.73$; $P < 0.0001$) across 3 cancer xenografts, thus providing a strong argument for specificity. A significantly different uptake pattern of ^{64}Cu -DOTA-AE105, compared with that of ^{18}F -FDG, was observed, thus emphasizing the additional information that can be obtained on tumor biology using ^{64}Cu -DOTA-AE105 PET. Furthermore, a significant correlation between baseline uPAR expression and sensitivity toward 5-fluorouracil was revealed, thus illustrating the possible potentials of uPAR PET in a clinical setting. **Conclusion:** Our results clearly demonstrate that the peptide-based PET tracer ^{64}Cu -DOTA-AE105 enables the noninvasive quantification of uPAR expression in tumors in vivo, thus emphasizing its potential use in a clinical setting to detect invasive cancer foci and for individualized cancer therapy.

Key Words: molecular imaging; uPAR; CD87; PET; cancer invasion; ^{64}Cu

J Nucl Med 2012; 53:138–145

DOI: 10.2967/jnumed.110.083386

In the case of solid tumors, it is the ability of cancer cells to invade the surrounding tissues and to form distant metastases that leads to progression and poor prognosis (1). Numerous studies have implicated the serine-protease urokinase-type plasminogen activator (uPA) (2) and its receptor (uPAR) to be of special importance in cancer invasion and metastasis (3), and uPAR is accordingly considered an attractive target for cancer therapy (4). Consistent with this role in cancer progression, high expression levels of uPAR have been shown to be strongly associated with metastatic disease and to correlate with poor prognosis in a variety of human malignancies such as breast, colorectal, and gastric cancer (5,6). Thorough studies by immunohistochemistry and in situ hybridization have revealed low expression levels of uPAR in normal homeostatic tissues, compared with malignant cancer lesions (7–9). The ability for detection of invasive cancers (9–12) makes the development of a noninvasive imaging modality to visualize and quantify uPAR expression in vivo attractive from a clinical, and in particular an oncologic, perspective.

Targeting uPAR with PET-based imaging probes in vivo has only recently been explored in a single pilot study (13). In that study, small-animal PET was performed in mice bearing uPAR-positive U87MG human glioblastomas and uPAR-negative MDA-MB-435 human breast cancer xenografts using a ^{64}Cu -labeled DOTA-conjugated small 9-mer peptide antagonist (^{64}Cu -DOTA-AE105) (Fig. 1) (13). A significantly higher accumulation in the uPAR-positive cell line than in the uPAR-negative cell line was found; however, no quantitative correlation between uPAR PET and uPAR expression levels, determined by established biochemical quantification methods in resected tumor tissues, was performed.

Received Jan. 13, 2011; revision accepted Aug. 17, 2011.

For correspondence or reprints contact: Andreas Kjaer, Department of Clinical Physiology, Nuclear Medicine and PET, Rigshospitalet KF-4012, Blegdamsvej 9, 2100, Copenhagen Ø, Denmark.

E-mail: akjaer@sund.ku.dk

COPYRIGHT © 2012 by the Society of Nuclear Medicine, Inc.

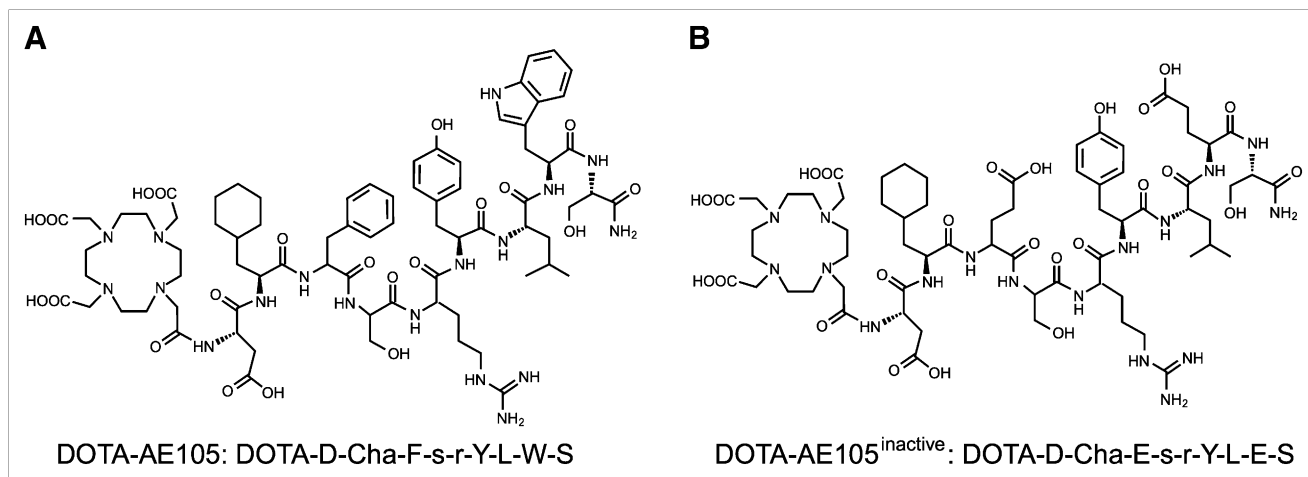


FIGURE 1. Chemical structures of DOTA-AE105 (A) and control peptide inactive DOTA-AE105 (B), in which 2 essential amino acids for uPAR binding (Phe → Glu and Trp → Glu) are substituted.

The present study therefore aims to investigate whether a quantitative relationship can be established between tracer uptake and uPAR expression in tumor tissues and furthermore illustrate the potential applications of such an imaging platform in a clinical setting using surrogate preclinical animal models. To enable this, we prepared ⁶⁴Cu-labeled AE105 conjugated to DOTA (⁶⁴Cu-DOTA-AE105) (13,14) and a nonbinding version (⁶⁴Cu-DOTA-AE105^{inactive}), with a comparable specific radioactivity as control. Quantitative PET images were recorded for a cohort of mice bearing xenotransplantations of 3 different human cancer cell lines selected for their different expression levels of uPAR. Furthermore, the tumor uptake of ⁶⁴Cu-DOTA-AE105 was also compared with ¹⁸F-FDG uptake in 2 different tumor types with high and low expression of uPAR. Finally, we illustrate the utility of the present uPAR-targeted PET as a possible surrogate response marker for conventional chemotherapy treatment in tumor-bearing mice.

MATERIALS AND METHODS

Chemical and Biologic Reagents

All commercial chemicals were of analytic grade. They were all used without further purification. Recombinant human uPAR and pro-uPA was produced and purified as described (15,16). A polyclonal rabbit anti-uPAR antibody was prepared in-house using purified recombinant uPAR expressed in Chinese hamster ovary cells as antigen (17). 2-(4,7,10-tris(2-tert-butoxy-2-oxoethyl)-1,4,7,10-tetraazacyclo-dodecan-1-yl)-acetic acid (DOTA-tris(tBu) ester) was purchased from CheMatech. ⁶⁴CuCl₂ in 0.1 M HCl was obtained from Risø, DTU. ¹⁸F-FDG was obtained from daily productions at the Department of Nuclear Medicine and PET, Copenhagen University Hospital.

Peptide Synthesis of DOTA-AE105 and Its Inactive Analog

Two 9-mer DOTA-conjugated peptides, AE105 (DOTA-Asp-Cha-Phe-(D)Ser-(D)Arg-Tyr-Leu-Trp-Ser-CONH₂) (Fig. 1A) and inactive AE105 (DOTA-Asp-Cha-Glu-(D)Ser-(D)Arg-Tyr-Leu-Glu-Ser-CONH₂) (Fig. 1B), were synthesized on Tentagel S RAM resin

(Rapp Polymere) using traditional Fmoc solid-phase peptide chemistry. In the final step, DOTA was coupled to the NH₂ terminus of the peptide on the resin by incubation with a 3-fold molar excess of DOTA-tris(tBu)ester for 24–48 h at room temperature. After deprotection and cleavage from the resin using 93% trifluoroacetic acid, 5% triisopropylsilane, and 2% H₂O for 6 h, the peptides were precipitated in diethylether and washed with diethylether 4 times. The dried peptides were purified by reversed-phase high-performance liquid chromatography and their integrity confirmed by matrix-assisted laser desorption ionization mass spectrometry (DOTA-AE105, 1,610.80 Da [mass difference, 0.01 Da] and inactive DOTA-AE105, 1,636.80 Da [mass difference, 0.07 Da]), where the deviation from the theoretic monoisotopic masses (MH⁺) are shown in brackets. Incubation of these peptides with a 2-fold molar excess of the stable Cu²⁺ at 5 mM led to complete complex formations of the DOTA-conjugated peptides as revealed by analytic reversed-phase high-performance liquid chromatography and matrix-assisted laser desorption ionization mass spectrometry (data not shown).

In Vitro Affinity Binding

The inhibitory concentration of 50% (IC₅₀) of these synthetic peptides for inhibition of the uPA•uPAR interaction were measured by surface plasmon resonance using a Biacore 3000 (GE Healthcare), performed as previously published (18). Subsequent fitting to the binding isotherms provided the IC₅₀ values of the different synthetic peptides.

Radiochemistry

The ⁶⁴Cu-labeled peptides, ⁶⁴Cu-DOTA-AE105 and inactive ⁶⁴Cu-DOTA-AE105, were radiosynthesized as previously described (13), with some modifications. In brief, 50 μL of ⁶⁴CuCl₂ (~150 MBq) in 0.1 M HCl was diluted in 450 μL of 0.1 M ammonium acetate (pH 8.0) containing 2 nmol of DOTA-conjugated peptide, followed by incubation at 70°C for 1 h. The ⁶⁴Cu-labeled peptide was subsequently purified using Sep-Pak Light C18 cartridges (Waters) and diluted with 8 volumes of water, ready for injection.

Cell Lines and Animal Models

All cells were obtained from the American Type Culture Collection, and all culture medium was obtained from Invitrogen Co.

All cell lines were cultured in standard medium supplemented with 10% (v/v) fetal bovine serum and 1% (v/v) penicillin–streptomycin at 37°C and 5% CO₂. Xenografts of human cancer cell lines were established by injection of 200 µL of cells (1 × 10⁸ cells/mL) suspended in 100 µL of Matrigel (BD Biosciences) subcutaneously in the left and right flanks of female NMRI nude mice obtained from Taconic, under anesthesia by Hypnorm (Fentanyl, 0.315 mg/mL + Fluanisone, 10 mg/mL) and Doricum (Midazolam, 5 mg/mL). When the tumor volume reached approximately 100–300 mm³ (2–3 wk after inoculation), the mice were enrolled in small-animal PET/CT studies. All animal experiments were performed under a protocol approved by the Animal Research Committee of the Danish Ministry of Justice.

Biodistribution Studies

Female nude mice bearing U87MG xenografts were injected in the tail vein with 2–3 MBq of ⁶⁴Cu-DOTA-AE105 or inactive ⁶⁴Cu-DOTA-AE105. All mice were euthanized at 4.5 h after tracer injection, and organs were resected for further analysis (i.e., wet weight). Blood, tumor, and major organs were collected, and the radioactivity was measured using a γ-counter from Perkin Elmer (*n* = 3 mice/group).

5-Fluorouracil Treatment Study

Twelve nude mice bearing the human colorectal carcinoma xenograft HT-29 in each flank were divided into 2 groups consisting of 6 animals each. All animals in each group were first PET/CT-scanned at baseline with ⁶⁴Cu-DOTA-AE105 (day 0). One group of 6 mice received saline on days 1 and 5, and the second group of 6 mice was dosed with 5-fluorouracil (50 mg/kg) on days 1 and 5. Subsequently, PET/CT of all mice in each group was repeated with ⁶⁴Cu-DOTA-AE105 on days 7 and 14 to assess the impact of 5-fluorouracil treatment on uPAR expression levels. Tumor volumes were measured by CT scanning on days 0, 7, and 14 using manual region-of-interest (ROI) drawing on the reconstructed images.

Small-Animal PET/CT

Ten-minute (1 and 4.5 h) and 20-min (22 h) PET scans were acquired with a microPET Focus 120 scanner (Siemens Medical Solutions). The energy window of the emission scans was set to 350–605 keV, with a time resolution of 6 ns. The acquired emission dataset was automatically stored in list mode. Small-animal PET studies were performed by intravenous injection of 5–7 MBq of either ⁶⁴Cu-DOTA-AE105 or inactive ⁶⁴Cu-DOTA-AE105 during sevoflurane anesthesia. A 10-min static PET scan was also obtained in the 5-fluorouracil treatment study at 1 h after injection of ⁶⁴Cu-DOTA-AE105. All list-mode data were postprocessed into 128 × 128 × 32 sinograms using 3-dimensional maximum a priori algorithms into 256 × 256 × 95 matrices with a voxel size of 0.43 mm³. The resolution of the PET scanner was 1.5 mm at the center of the field of view and 1.8 mm at 38 mm off-center using 3-dimensional maximum a priori. CT data were acquired with a MicroCAT II tomograph (Siemens Medical Solutions). The radiographic tube with a 0.5-mm aluminum filter was set at 40 kVp, a tube current of 500 µA, and an exposure time of 700 ms per projection. The pixel size was 0.095 × 0.095 × 0.095 mm. All results were analyzed using Inveon software (Siemens Medical Solutions) and expressed as percentage injected dose per gram of tissue (%ID/g). Immediately after the PET scan, the animals were sacrificed by decapitation. Tumors were rapidly

resected and placed in a –80°C freezer for subsequent uPAR enzyme-linked immunosorbent assay (ELISA) analysis.

Extraction of uPAR from Resected Tumor Tissue

Resected tumors were precooled in liquid nitrogen, pulverized, and weighed. Then, proteins were extracted in ice-cold 1% Triton X-114 (Sigma-Aldrich) in phosphate-buffered saline (19), at a ratio of 1:10 (v/v), followed by centrifugation for 30 min at 10,000g at 4°C to remove insoluble cell debris (19). The uPAR-containing supernatant was collected and heated to 37°C to induce detergent-phase separation. The uPAR-enriched detergent phase was collected by centrifugation at 2,000g for 5 min and subsequently used for quantification of its uPAR content by ELISA.

Quantification of uPAR by ELISA

Quantitative assessment of uPAR in tumor lysates was performed by ELISA as previously described, with some modifications (20). The ELISA plates were washed and subsequently incubated for 120 min with binding buffer (100 µL/well) containing purified uPAR (1 ng/mL) or tumor extracts diluted to 1:10 (v/v) in assay buffer. After additional washings, the bound uPAR was detected by incubation for 60 min with 100 µL of the monoclonal uPAR antibody R2 (1.0 µg/mL), followed by washings and incubation for 30 min with 100 µL of horseradish peroxidase–conjugated secondary antibody diluted to 1:2,000 (v/v). The bound horseradish peroxidase activity was quantified by a 20-min reaction with 0.1% (v/v) *o*-phenylenediamine (100 µL/well) and 0.01% (v/v) H₂O₂ in 0.1% (v/v) citrate-phosphate buffer, pH 5.0. The reaction was stopped by addition of 100 µL of 1 M H₂SO₄, and absorbance was read at 492 nm. All samples were measured in duplicate in 2 separate studies. Mean values for the 2 studies were used in the correlation. All washings were performed 6 times with phosphate-buffered saline using a Nunc Immuno-washer (Thermo Scientific). All procedures were performed at room temperature.

Immunohistochemistry

uPAR immunostaining was performed as previously published (7), with minor modifications. In short, paraffin-embedded tissue sections (3 µm) were deparaffinized and subjected to antigen retrieval by proteinase K (10 µg/mL) treatment for 25 min at 37°C. Endogenous peroxidase activity was blocked by incubation in 1% (v/v) hydrogen peroxide water solution for 15 min. The primary rabbit polyclonal antibody against human uPAR (17) was diluted in antibody diluent (S3022; Dako) and incubated overnight in Shandon racks (Thermo Shandon) at a concentration of 1.8 µg/mL. Subsequently, the primary antibodies were detected with EnVision reagent (Dako), with antirabbit IgG horseradish peroxidase–conjugated polymers (K4003; Dako). The reactions were visualized by incubating the sections with NovaRED (Vector Laboratories) according to the manufacturer's instructions and counterstained with Mayer hematoxylin. The specificity of the immunohistochemical staining was validated either by replacing the primary antibody with purified rabbit IgG of irrelevant specificity or by adding purified uPAR (3.3 µg/mL) to the primary rabbit anti-uPAR antibody (molar ratio between monoclonal antibody and recombinant uPAR was 1:100), which in both cases reassuringly eliminated the observed staining (not shown).

Statistical Analysis

Quantitative data are expressed as mean ± SEM, and means are compared using 1-way ANOVA. Correlation statistics were per-

formed using linear regression analysis. *P* values of 0.05 or less were considered statistically significant.

RESULTS

Impact of DOTA Conjugation on Targeting Affinity

The interactions of AE105, DOTA-AE105, and inactive DOTA-AE105 (Fig. 1) with immobilized human uPAR were measured in real time by surface plasmon resonance. No reduction in the efficacy to compete the uPA • uPAR interaction because of the DOTA conjugation (AE105: IC₅₀, 11 nM, vs. DOTA-AE105: IC₅₀, 7 nM) (Supplemental Fig. 1A; supplemental materials are available online only at <http://jnm.snmjournals.org>) was found, indicating that the addition of the DOTA chelator group had no effect on the uPAR binding affinity. The 2 nonconservative replacements of hot-spot residues (i.e., Phe → Glu and Trp → Glu, Fig. 1A), selected on structural–functional considerations (21), led to a significant reduction in affinity for the corresponding nonbinding control peptide inactive DOTA-AE105, which presents an IC₅₀ of 78 μM.

Radiochemistry

⁶⁴Cu labeling of DOTA-AE105 and inactive DOTA-AE105 was achieved in high yield (>90%) and with a radiochemical purity greater than 95% (Supplemental Fig. 1B) after Sep-Pak purification. A relatively high specific activity of approximately 25 GBq/μmol was obtained for both ⁶⁴Cu-DOTA-AE105 and inactive ⁶⁴Cu-DOTA-AE105 at the end of the synthesis (decay-corrected), with a radioactivity concentration of 30 MBq/mL.

Biodistribution Studies

In vivo biodistribution studies were performed for ⁶⁴Cu-DOTA-AE105 and inactive ⁶⁴Cu-DOTA-AE105 to evaluate their baseline distributions in major murine organs and to validate the small-animal PET quantification measured in parallel (Fig. 2). Both radiolabeled peptides cleared rapidly from the bloodstream, primarily via the hepatic–intestinal route. The tumor uptake of ⁶⁴Cu-DOTA-AE105 was 4.2% ± 0.8 %ID/g, whereas uptake in blood and muscle was 1.2% ± 0.1 %ID/g and 0.3% ± 0.1 %ID/g, respectively, thus generating a tumor-to-blood and tumor-to-muscle ratio of 3.5 and 16, respectively. The tumor uptake of the control peptide inactive ⁶⁴Cu-DOTA-AE105 at 4.5 h, compared with ⁶⁴Cu-DOTA-AE105, was significantly reduced to 1.7% ± 0.9 %ID/g (*P* = 0.0243), thus substantiating the specificity of ⁶⁴Cu-DOTA-AE105 toward human uPAR. Uptake of inactive ⁶⁴Cu-DOTA-AE105 in blood and muscle was 1.4% ± 0.5 %ID/g and 0.4% ± 0.1 %ID/g, respectively, and was not significantly different from ⁶⁴Cu-DOTA-AE105. The highest uptake for both labeled peptides was observed in the liver, with values of 14% ± 2 %ID/g and 11 ± 2 %ID/g, for ⁶⁴Cu-DOTA-AE105 and inactive ⁶⁴Cu-DOTA-AE105, respectively.

Small-Animal PET/CT Study

In the first line of experiments, a group of U87MG tumor-bearing mice was PET-scanned at 1, 4.5, and 22 h

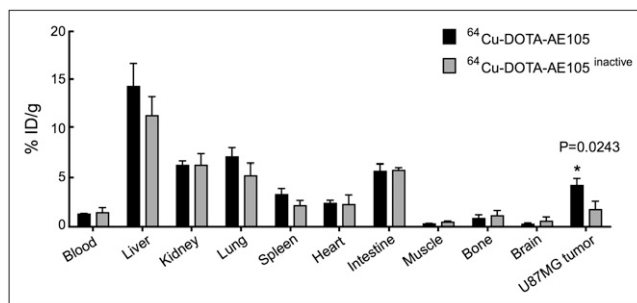


FIGURE 2. Biodistribution results for ⁶⁴Cu-DOTA-AE105 and inactive ⁶⁴Cu-DOTA-AE105 in nude mice bearing subcutaneously xenotransplanted U87MG human glioblastoma at 4.5 h after injection. Results are shown as %ID/g ± SEM (*n* = 3 mice/group).

after intravenous injection with ⁶⁴Cu-DOTA-AE105, inactive ⁶⁴Cu-DOTA-AE105, or ⁶⁴Cu-DOTA-AE105, after a bolus dose of unlabeled DOTA-AE105 (30 μg) (blocking) 5 min before the PET tracer was administered. Representative images of the transverse planes for each group of mice at 4.5 h after injection are shown in Figure 3A, with the corresponding ROI-based quantitative tumor uptake levels in shown in Figure 3B. A significantly higher tumor uptake for ⁶⁴Cu-DOTA-AE105 than for either the control peptide (inactive ⁶⁴Cu-DOTA-AE105) group or the blocking-dose group (*n* = 3, *P* < 0.001) was observed at all 3 times. At 4.5 h after injection, the uptake was 5.9% ± 0.7 %ID/g, 2.2% ± 0.2 %ID/g, and 1.3% ± 0.1 %ID/g for the ⁶⁴Cu-DOTA-AE105, inactive ⁶⁴Cu-DOTA-AE105, and blocking groups, respectively.

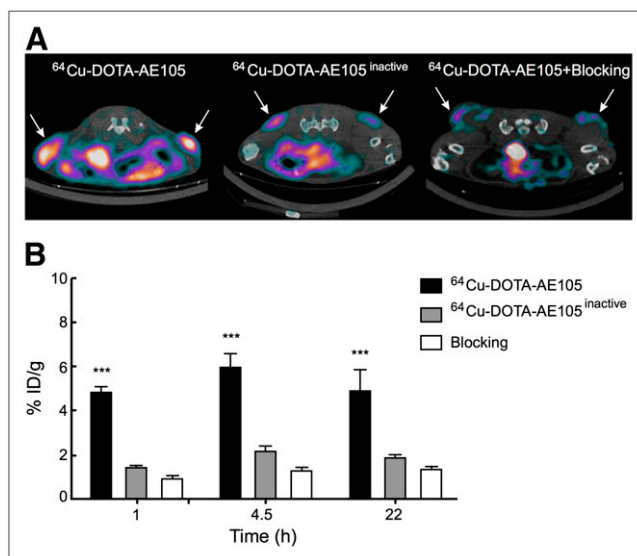


FIGURE 3. Representative decay-corrected transverse images at 4.5 h after injection of ⁶⁴Cu-DOTA-AE105, inactive ⁶⁴Cu-DOTA-AE105, and ⁶⁴Cu-DOTA-AE105 preinjected with excess of DOTA-AE105 (blocking) (A). Representative images shown are static scans of single mouse (arrows indicate tumors), which is representative of 3 mice tested in each group, with corresponding quantitative tumor ROI analysis (B). Results are shown as %ID/g ± SEM (*n* = 3 mice/group).

To correlate the tumor uptake of ^{64}Cu -DOTA-AE105 with uPAR expression, 3 different human cancer xenograft models were analyzed in a second line of experiments. ELISA on detergent-phase extracts from whole tumor lysates revealed the uPAR expression levels in H727, HT-29, and U87MG to be 26 ± 2 , 62 ± 8 , and 100 ± 9 pg/mg, respectively (Supplemental Fig. 2A). The relative ranking of expression levels was roughly comparable to that observed by immunohistochemical staining for human uPAR on tumor slides from the same xenotransplantations (Supplemental Figs. 2B–2D). Static small-animal PET/CT scans were obtained on all 3 tumor xenograft models, and representative transverse images after tail vein injection of ^{64}Cu -DOTA-AE105 are shown in Figure 4A. Scans were obtained at 1, 4.5, and 22 h after injection ($n = 4$ per group). The tumors were clearly visible in all 3 xenograft models. A significant correlation between tumor uptake of ^{64}Cu -DOTA-AE105 and uPAR expression was observed at 1.0 h after injection ($P < 0.0001$, $R^2 = 0.73$, Fig. 4B). This correlation was maintained at 4.5 h ($P < 0.0002$, $R^2 = 0.65$) and 22 h ($P = 0.01$, $R^2 = 0.43$) after injection.

In a third line of experiments, 10-min static PET scans at 1 h after injection of either ^{18}F -FDG or ^{64}Cu -DOTA-AE105 were acquired in 3 mice bearing the high uPAR-expressing xenograft U87MG on the right flank and the low express-

ing-uPAR xenograft H727 on the left flank. Representative transverse images are shown in Figure 5A. A clearly visible difference in tumor uptake of ^{64}Cu -DOTA-AE105 was seen between the 2 tumor transplantations, whereas no difference in uptake was observed for ^{18}F -FDG. This finding was confirmed in a quantitative ROI analysis, in which no significant difference in ^{18}F -FDG tumor uptake was found between the 2 tumor models (Fig. 5B), with H727 and U87MG having an ^{18}F -FDG uptake of $1.52\% \pm 0.03$ %ID/g and $1.97\% \pm 0.18$ %ID/g, respectively. In contrast, a significant difference was observed for ^{64}Cu -DOTA-AE105 ($P < 0.05$), with H727 and U87MG having uptake values of $1.71\% \pm 0.11$ %ID/g and $3.88\% \pm 0.74$ %ID/g, respectively.

During these studies, we observed that PET of xenotransplantations originating from the colorectal cancer cell line HT-29 consistently revealed a circular appearance in the accumulation of the ^{64}Cu -DOTA-AE105 tracer in the tumor (Figs. 4A and 6A). This morphology is distinctly different from the one observed for the glioblastoma cell line U87MG, which revealed a general tracer accumulation throughout the transplantation, with higher levels located centrally (Figs. 4A and 6B). This distinct uptake pattern prompted us to perform a subsequent analysis for uPAR

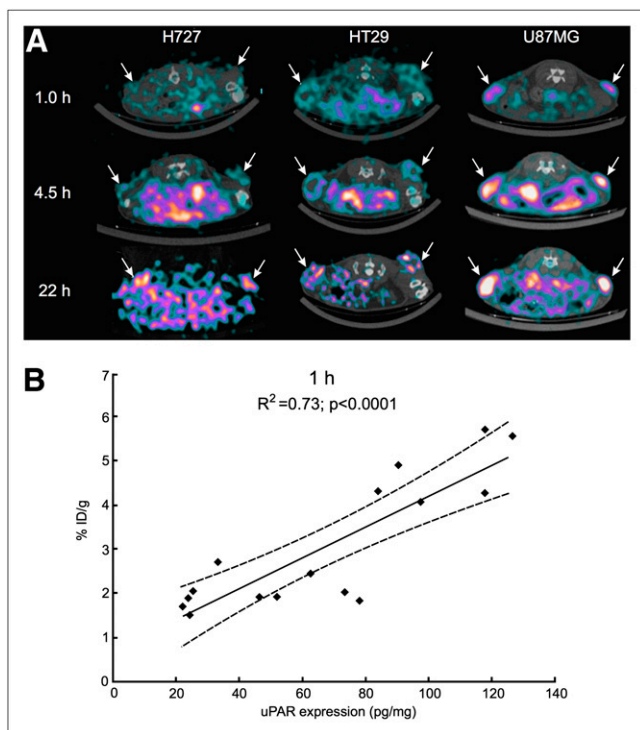


FIGURE 4. Decay-corrected transverse images of subcutaneously xenotransplanted U87MG, HT-29, and H727 mice at 1, 4.5, and 22 h after injection of ^{64}Cu -DOTA-AE105 (A). Images shown are static scans of single mouse, which is representative of 4 mice tested in each group. Arrows indicate tumors. Correlation between tumor uptake at 1 h after injection of ^{64}Cu -DOTA-AE105 (%ID/g) and corresponding uPAR expression (pg/mg) is depicted ($n = 16$ tumors) (B).

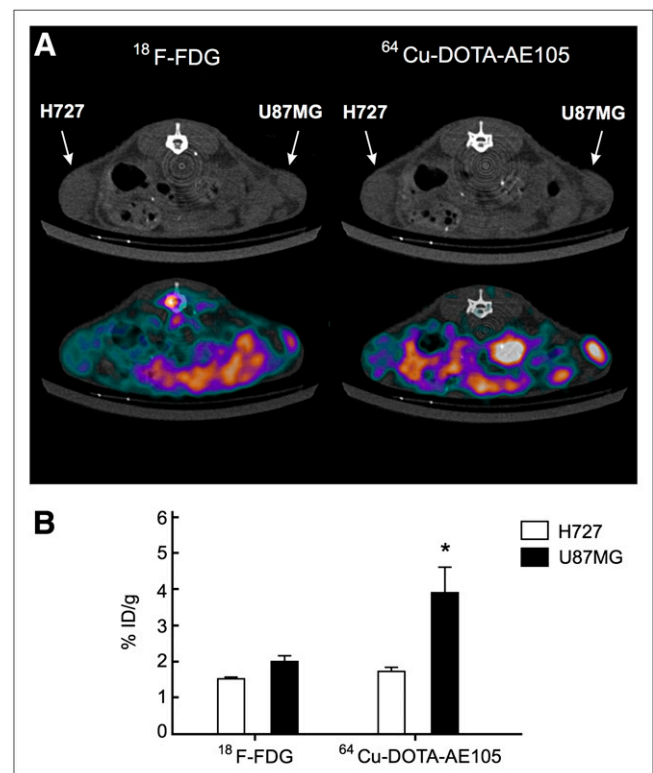


FIGURE 5. Representative decay-corrected coronal (top) and transversal (bottom) images of same mouse at 1 h after injection of either ^{18}F -FDG or ^{64}Cu -DOTA-AE105 (A). Mouse was inoculated with 2 different xenotransplanted tumors on each flank (H727 and U87MG). Arrows indicate tumor. Comparison of quantified tumor uptake of ^{18}F -FDG and ^{64}Cu -DOTA-AE105 in 3 combination mice bearing two different human cancer xenografts (combi-mice) is shown. Results are shown as %ID/g \pm SEM ($n = 3$) (B).

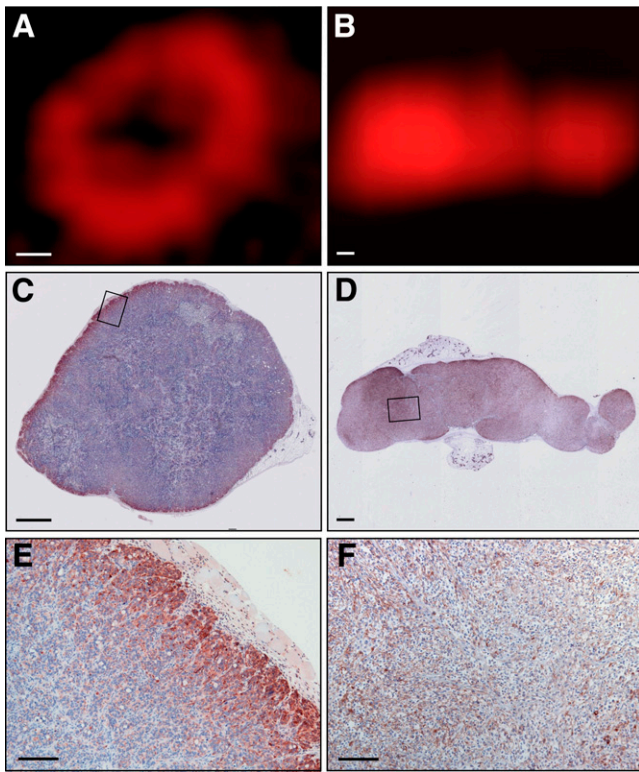


FIGURE 6. High-resolution uPAR PET images of tumor and corresponding immunohistologic slides for HT-29 (A, C, and E) and U87MG (B, D, and F). One tumor for each type was PET-scanned and afterward resected and stained for human uPAR. High degree of correlation between uPAR expression pattern and uptake of ^{64}Cu -DOTA-AE105 in each tumor was observed. Bar = 1 mm in A–D and 40 μm in E–F.

expression at higher resolutions by immunohistochemistry of the corresponding tumors. Interestingly, closely matching patterns were found between uPAR expression and PET tracer uptake for both cancer cell lines (Fig. 6). Furthermore, the HT-29 colon cancer line appears to recapitulate the general expression observed in human colorectal cancer (7), with the uPAR expression in the xenotransplantation being confined to a few cell layers facing the mouse stoma. Overall, this expression pattern analysis provides strong independent evidence for the specificity of ^{64}Cu -DOTA-AE105.

Finally, to illustrate the potential clinical value of quantitative uPAR PET, a treatment study using 5-fluorouracil on the colorectal xenograft model was performed. 5-fluorouracil constitutes the cornerstone modality in the chemotherapeutic treatment of colon cancer patients in the clinic. Using our quantitative uPAR PET platform, we were actually able to demonstrate a correlation between high levels of uPAR expression at baseline (day 0) and a decreased response to treatment with 5-fluorouracil on day 7 ($P = 0.05$, $R^2 = 0.32$) (Fig. 7). At day 14, the tumors in the control group presented an average size of $224.1 \pm 27.8 \text{ mm}^3$, whereas that of the 5-fluorouracil-challenged group was only $165.9 \pm 23.8 \text{ mm}^3$ (data not shown), thus confirming the efficacy of 5-fluorouracil on tumor growth.

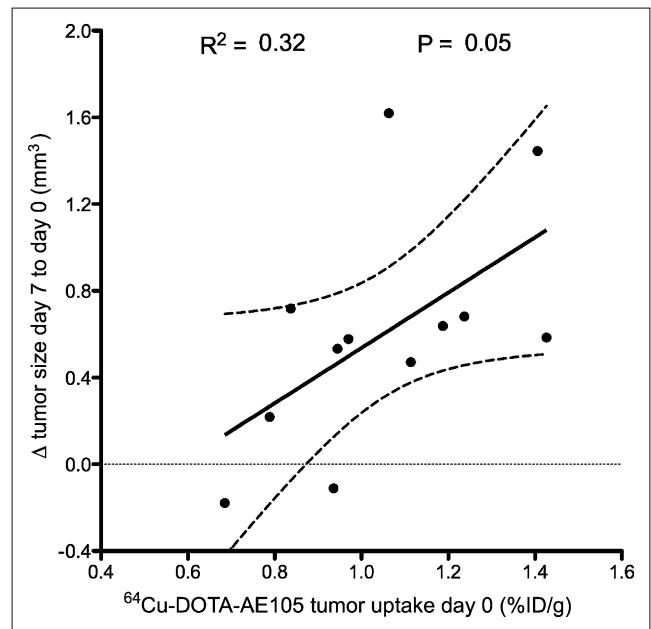


FIGURE 7. Correlation between baseline uPAR expression levels detected by ^{64}Cu -DOTA-AE105 PET at day 0 and sensitivity toward 5-fluorouracil chemotherapy treatment ($P = 0.05$, $r^2 = 0.32$) in nude mice bearing human colorectal HT-29 cancer xenografts ($n = 12$ tumors).

DISCUSSION

This study shows, to the best of our knowledge, the first evidence of a quantitative correlation between tumor accumulation of a uPAR-targeting PET tracer and uPAR expression levels across multiple human cancer xenograft mouse models. In addition, we provide the first example for a possible clinical impact of this new PET tracer using a surrogate mouse model. Collectively, these results clearly encourage further development of ^{64}Cu -DOTA-AE105 for PET of uPAR of invasive cancers in various malignancies in patients.

PET of uPAR holds great promise for improving the survival of patients with invasive cancers. Extensive studies and documentation exist, in which high levels of uPAR in either plasma or tumor biopsies implicate a negative prognosis in several types of cancer (22,23). A PET tracer detecting invasive or chemotherapy-resistant cancers at an early time point could, therefore, have great impact for selection of treatment strategy and thereby prognosis. In addition, if a future uPAR-targeted therapy should be introduced into the clinic, identification of patients with local high uPAR expression levels in the tumor microenvironment could increase the chances for successful intervention. Such uPAR-targeted therapies based on monoclonal antibodies, peptide antagonists, or protease-activated prodrugs are currently being investigated in several preclinical cancer models (24–26).

The development of uPAR-targeting PET probes for non-invasive imaging of uPAR has only recently been reported (13). A small 9-mer peptide antagonist we developed by combinatorial chemistry (14) was used both in the present and in the preceding study to achieve uPAR-specific targeting.

The first study (13) reported, however, a 2-fold higher tumor uptake (10.8 ± 1.5 %ID/g) than did the present study, although the same uPAR-positive U87MG cell line was used. The reason for this difference in the absolute uptake values is presently unknown but may pertain to differences in uPAR expression between the cell lines or differences in the specific activity of the tracer. The latter possibility is favored by the observation that the 2-fold difference between the studies was maintained for the nonbinding control peptide, indicating that the discrepancy is not related to the targeting event per se but rather reflects unrelated properties of the chelated radionuclide.

Our *in vivo* biodistribution data did nevertheless show a relatively high liver uptake, with values of $14.2\% \pm 2.4$ %ID/g for ^{64}Cu -DOTA-AE105 at 4.5 h after injection (Fig. 2). Such high liver uptake is also reported in other studies using DOTA as a chelator for ^{64}Cu (27,28). One likely explanation for this high liver uptake is the established *in vivo* instability of the ^{64}Cu -DOTA complex due to transchelation of the metal to superoxide dismutase in the liver or transmetalation with various metals *in vivo* (29–31). In the present study, we concordantly found a significant correlation ($R^2 = 0.73$; $P < 0.0001$) already at 1.0 h after injection (Fig. 4B), with a somewhat decreasing correlation over time (4.5 h: $R^2 = 0.65$ and $P = 0.0002$, 22 h: $R^2 = 0.43$ and $P = 0.01$), thus indicating that the stability of the ^{64}Cu -DOTA-AE105 complex is indeed an issue for further improvement in the present experimental setup. Importantly, improved macrocyclic chelators have been developed, including 1,4,8,11-tetraazacyclotetradecane-1,4,8,11-tetraacetic acid and various cross-bridge tetraazamacrocycles, which have demonstrated a remarkably good *in vivo* stability (32). As reviewed recently (33), the structure of human uPAR solved in complex with an AE105 derivative (34) clearly suggests that there is ample free conformational space in this complex, allowing relatively large NH_2 -terminal modifications of the core peptide (AE105) without impairing the stability of the corresponding complex. We are thus currently exploring these new chelators with the aim of improving the target-to-nontarget ratio and to reduce the relatively high liver uptake we observed using ^{64}Cu -DOTA-AE105 in particular.

Several receptor-based targets for PET have been investigated in the last decade, with the integrins human epidermal growth factor receptor 2 and vascular endothelial growth factor being some of the more successful receptor-based targets (35). The main clinical application for these PET tracers is to aid in the selection of those patients who may benefit from such intervention therapies targeting the receptors in question. However, strict evaluations of quantitative correlations between the target expression level *in vivo* and the PET data are so far scarce. The variable basal expression levels of most biologic target proteins emphasize the relevance of such quantitative PET data. Although the basal expression levels of uPAR in various homeostatic tissues generally are considered to be low, a quantitative assessment of the PET signal may nevertheless facilitate the

confinement of the tumor lesion site and surrounding reactive stroma using properly assigned cutoff values. These values need, however, to be defined empirically in the clinic.

In this study, we have demonstrated that we specifically can detect and assess the levels of human uPAR expression in 3 subcutaneous implanted human cancer xenografts in mice. However, the subcutaneous xenotransplantation tumor model used in this study does not, of course, accurately mimic the histology and stromal interactions seen in cancer patients. In addition, this model does not in fact reveal the baseline uPAR expression in the murine host tissues, because of the species selectivity of the core peptide AE105 for human uPAR (16). Therefore, the true biodistribution patterns and targeting properties remain to be evaluated in patients.

The results presented in this study not only provide evidence of the first quantitative relationship between tumor uptake of ^{64}Cu -DOTA-AE105 and uPAR expression but also open up new possibilities for further studies. Given the substantial number of published studies relating high uPAR expression to poor prognosis in a variety of human cancers, it seems obvious to use ^{64}Cu -DOTA-AE105 for PET at the time of diagnosis as a supplement to standard ^{18}F -FDG PET. Besides the new information achieved, as illustrated in Figure 5, primary tumor uptake of this tracer apparently correlates to the efficacy of 5-fluorouracil-based chemotherapies, as illustrated in Figure 7. Intriguingly, a similar correlation has previously been reported for various small-cell lung cancer cell lines (36). Another recently published study implicates that the expression of uPAR could be a biomarker of sensitivity toward cetuximab treatment (37), in which high levels of uPAR expression conferred resistance to cetuximab treatment in non-small-cell lung cancer patients.

CONCLUSION

The results in this study provide the first, to our knowledge, evidence of the quantitative relationship between tumor uptake of the uPAR-specific PET tracer ^{64}Cu -DOTA-AE105 and uPAR expression *in vivo*. Given the substantial amount of published studies showing uPAR to be expressed at the invasive front in a variety of cancers and as a biomarker for sensitivity for various chemotherapies, it seems promising to use ^{64}Cu -DOTA-AE105 for PET of uPAR expression in several cancers in the clinic.

DISCLOSURE STATEMENT

The costs of publication of this article were defrayed in part by the payment of page charges. Therefore, and solely to indicate this fact, this article is hereby marked “advertisement” in accordance with 18 USC section 1734.

ACKNOWLEDGMENTS

We thank Gitte Juhl Funch, Lotte A. Frederiksen, and John Post for excellent technical assistance. This work was supported by the Danish National Research Foundation (Centre

for Proteases and Cancer), Danish Medical Research Council, Danish National Advanced Technology Foundation, Novo Nordisk Foundation, Lundbeck Foundation, and A.P. Moeller Foundation. No other potential conflict of interest relevant to this article was reported.

REFERENCES

1. Sporn MB. The war on cancer. *Lancet*. 1996;347:1377–1381.
2. Schmitt M, Mengele K, Napieralski R, et al. Clinical utility of level-of-evidence-1 disease forecast cancer biomarkers uPA and its inhibitor PAI-1. *Expert Rev Mol Diagn*. 2010;10:1051–1067.
3. Jacobsen B, Ploug M. The urokinase receptor and its structural homologue C4.4A in human cancer: expression, prognosis and pharmacological inhibition. *Curr Med Chem*. 2008;15:2559–2573.
4. Romer J, Nielsen BS, Ploug M. The urokinase receptor as a potential target in cancer therapy. *Curr Pharm Des*. 2004;10:2359–2376.
5. Foekens JA, Peters HA, Look MP, et al. The urokinase system of plasminogen activation and prognosis in 2780 breast cancer patients. *Cancer Res*. 2000;60:636–643.
6. Rasch MG, Lund IK, Almasi CE, Hoyer-Hansen G. Intact and cleaved uPAR forms: diagnostic and prognostic value in cancer. *Front Biosci*. 2008;13:6752–6762.
7. Illemann M, Bird N, Majeed A, et al. Two distinct expression patterns of urokinase, urokinase receptor and plasminogen activator inhibitor-1 in colon cancer liver metastases. *Int J Cancer*. 2009;124:1860–1870.
8. Nielsen BS, Rank F, Illemann M, Lund LR, Dano K. Stromal cells associated with early invasive foci in human mammary ductal carcinoma in situ coexpress urokinase and urokinase receptor. *Int J Cancer*. 2007;120:2086–2095.
9. Dublin E, Hanby A, Patel NK, Liebman R, Barnes D. Immunohistochemical expression of uPA, uPAR, and PAI-1 in breast carcinoma: fibroblastic expression has strong associations with tumor pathology. *Am J Pathol*. 2000;157:1219–1227.
10. Jankun J, Merrick HW, Goldblatt PJ. Expression and localization of elements of the plasminogen activation system in benign breast disease and breast cancers. *J Cell Biochem*. 1993;53:135–144.
11. Costantini V, Sidoni A, Deveglio R, et al. Combined overexpression of urokinase, urokinase receptor, and plasminogen activator inhibitor-1 is associated with breast cancer progression: an immunohistochemical comparison of normal, benign, and malignant breast tissues. *Cancer*. 1996;77:1079–1088.
12. Fisher JL, Field CL, Zhou H, Harris TL, Henderson MA, Choong PF. Urokinase plasminogen activator system gene expression is increased in human breast carcinoma and its bone metastases—a comparison of normal breast tissue, non-invasive and invasive carcinoma and osseous metastases. *Breast Cancer Res Treat*. 2000;61:1–12.
13. Li ZB, Niu G, Wang H, et al. Imaging of urokinase-type plasminogen activator receptor expression using a ^{64}Cu -labeled linear peptide antagonist by microPET. *Clin Cancer Res*. 2008;14:4758–4766.
14. Ploug M, Ostergaard S, Gardsvoll H, et al. Peptide-derived antagonists of the urokinase receptor: affinity maturation by combinatorial chemistry, identification of functional epitopes, and inhibitory effect on cancer cell intravasation. *Biochemistry*. 2001;40:12157–12168.
15. Jacobsen B, Gardsvoll H, Juhl Funch G, Ostergaard S, Barkholt V, Ploug M. One-step affinity purification of recombinant urokinase-type plasminogen activator receptor using a synthetic peptide developed by combinatorial chemistry. *Protein Expr Purif*. 2007;52:286–296.
16. Lin L, Gardsvoll H, Huai Q, Huang M, Ploug M. Structure-based engineering of species selectivity in the interaction between urokinase and its receptor: implication for preclinical cancer therapy. *J Biol Chem*. 2010;285:10982–10992.
17. Rønne E, Hoyer-Hansen G, Brunner N, et al. Urokinase receptor in breast cancer tissue extracts: enzyme-linked immunosorbent assay with a combination of mono- and polyclonal antibodies. *Breast Cancer Res Treat*. 1995;33:199–207.
18. Gaardsvoll H, Jacobsen B, Kriegbaum MC, et al. Conformational regulation of urokinase receptor (uPAR) function: impact of receptor occupancy and epitope-mapped monoclonal antibodies on lamellipodia induction. *J Biol Chem*. 2011;286:33544–33556.
19. Ploug M, Ronne E, Behrendt N, Jensen AL, Blasi F, Dano K. Cellular receptor for urokinase plasminogen activator: carboxyl-terminal processing and membrane anchoring by glycosyl-phosphatidylinositol. *J Biol Chem*. 1991;266:1926–1933.
20. Riisbro R, Christensen IJ, Piironen T, et al. Prognostic significance of soluble urokinase plasminogen activator receptor in serum and cytosol of tumor tissue from patients with primary breast cancer. *Clin Cancer Res*. 2002;8:1132–1141.
21. Ploug M. Structure-function relationships in the interaction between the urokinase-type plasminogen activator and its receptor. *Curr Pharm Des*. 2003;9:1499–1528.
22. de Bock CE, Wang Y. Clinical significance of urokinase-type plasminogen activator receptor (uPAR) expression in cancer. *Med Res Rev*. 2004;24:13–39.
23. Dass K, Ahmad A, Azmi AS, Sarkar SH, Sarkar FH. Evolving role of uPA/uPAR system in human cancers. *Cancer Treat Rev*. 2008;34:122–136.
24. Knör S, Sato S, Huber T, et al. Development and evaluation of peptidic ligands targeting tumour-associated urokinase plasminogen activator receptor (uPAR) for use in alpha-emitter therapy for disseminated ovarian cancer. *Eur J Nucl Med Mol Imaging*. 2008;35:53–64.
25. Rabbani SA, Ateeq B, Arakelian A, et al. An anti-urokinase plasminogen activator receptor antibody (ATN-658) blocks prostate cancer invasion, migration, growth, and experimental skeletal metastasis in vitro and in vivo. *Neoplasia*. 2010;12:778–788.
26. Schafer JM, Peters DE, Morley T, et al. Efficient targeting of head and neck squamous cell carcinoma by systemic administration of a dual uPA and MMP-activated engineered anthrax toxin. *PLoS ONE*. 2011;6:e20532.
27. Wu Y, Zhang X, Xiong Z, et al. microPET imaging of glioma integrin $\alpha_3\beta_3$ expression using ^{64}Cu -labeled tetrameric RGD peptide. *J Nucl Med*. 2005;46:1707–1718.
28. Miao Z, Ren G, Liu H, Jiang L, Cheng Z. Small-animal PET imaging of human epidermal growth factor receptor positive tumor with a ^{64}Cu labeled affibody protein. *Bioconjug Chem*. 2010;21:947–954.
29. Bass LA, Wang M, Welch MJ, Anderson CJ. In vivo transchelation of copper-64 from TETA-octreotide to superoxide dismutase in rat liver. *Bioconjug Chem*. 2000;11:527–532.
30. Cole WC, DeNardo SJ, Meares CF, et al. Serum stability of ^{67}Cu chelates: comparison with ^{111}In and ^{57}Co . *Int J Rad Appl Instrum B*. 1986;13:363–368.
31. Boswell CA, Sun X, Niu W, et al. Comparative in vivo stability of copper-64-labeled cross-bridged and conventional tetraazamacrocyclic complexes. *J Med Chem*. 2004;47:1465–1474.
32. Anderson CJ, Wadas TJ, Wong EH, Weisman GR. Cross-bridged macrocyclic chelators for stable complexation of copper radionuclides for PET imaging. *Q J Nucl Med Mol Imaging*. 2008;52:185–192.
33. Kriegbaum MC, Persson M, Haldager L, et al. Rational targeting of the urokinase receptor (uPAR): development of inhibitors and non-invasive imaging probes. *Curr Drug Targets*. 2011;12:1711–1728.
34. Llinas P, Le Du MH, Gardsvoll H, et al. Crystal structure of the human urokinase plasminogen activator receptor bound to an antagonist peptide. *EMBO J*. 2005;24:1655–1663.
35. Chen K, Chen X. Positron emission tomography imaging of cancer biology: current status and future prospects. *Semin Oncol*. 2011;38:70–86.
36. Gutova M, Najbauer J, Gevorgyan A, et al. Identification of uPAR-positive chemoresistant cells in small cell lung cancer. *PLoS ONE*. 2007;2:e243.
37. Nikolova DA, Asangani IA, Nelson LD, et al. Cetuximab attenuates metastasis and u-PAR expression in non-small cell lung cancer: u-PAR and E-cadherin are novel biomarkers of cetuximab sensitivity. *Cancer Res*. 2009;69:2461–2470.